Photocatalytic Degradation of Rhodamine B and Methylene blue Using α-Fe$_2$O$_3$ Nanoparticles

S. Abdalkareem Jasim[a], M.M. Kadhim[b,c], B. Abed Hussein[d], S. Emad Izzat[e], Z. Mohsen Najm[f] and C. Chem[g],*

[a]*Al-maarif University College, Medical Laboratory Techniques Department, Al-Anbar-Ramadi, Iraq*
[b]*Department of Medical Laboratory Techniques, Dijlah University College, Baghdad, 10021, Iraq*
[c]*Medical Laboratory Techniques Department, Al-Farahidi University, Baghdad, Iraq*
[d]*Al-Manara College for Medical Sciences, Misan, Iraq*
[e]*Al-Nisour University College, Baghdad, Iraq*
[f]*Anesthesia Techniques Department, Al-Mustaqbal University College, Babylon, Iraq*
[g]*Department of Chemistry, Xian University, Xian, China*

In this work, hematite (α-Fe$_2$O$_3$) nanoparticles were prepared using wet chemical approach accompanied by thermal decomposition and were characterized using Fourier transform infrared (FT-IR) spectroscopy, powder X-ray diffraction (XRD), vibrating sample magnetometer (VSM) and transmission electron microscope (TEM). The FT-IR and XRD results confirm that the successful preparation of pure hematite α-Fe$_2$O$_3$. The VSM predicts the ferromagnetic behavior for as-prepared α-Fe$_2$O$_3$. The TEM image shows that the particles are separated, not agglomerated with quasi-spherical shape. Also, the particles are less than 100 nm. In addition, photo-degradation of rhodamine B (RhB) and methylene blue (MB) dyes was studied using α-Fe$_2$O$_3$ nanoparticles under visible light.

INTRODUCTION

Different organic natural and synthetic dyes with high aromaticity, complex structure, stability, solubility, and low biodegradability used in various industries are major water pollutions in recent years and causes various damage to humans and other organisms [1-18]. Therefore, the removal of organic dyes from industrial wastewaters before discharge to the environment is urgent and necessary using different techniques such as adsorption [1-4] and photocatalytic degradation [5-11]. Advanced oxidation processes (AOP) using various catalyst such as zinc ferrite [12], Bi$_2$O$_3$/SrFe$_{12}$O$_{19}$ [13], TiO$_2$/ZnO [14], graphene/CeO$_2$ [15], Ag/TiO$_2$/biochar [16], Fe$_3$O$_4$@SiO$_2$@CeO$_2$ [17],

CeO$_2$/Bi$_2$WO$_6$ [18] are very used to degraded different organic dyes in aqueous solution. Upon photocatalyst irradiated by UV and/or Visible light, electrons excited from the valence band (VB) to the conductive band (CB) to form very reactive electron-hole pair. The h$^+_{VB}$ and e$^-_{CB}$ reacted to H$_2$O and O$_2$ molecules to prepare hydroxyl (OH°) and oxygen (O$_2$°) radicals. Finally, these radicals attached to organic dyes and degraded them to safety molecules [12-18]. In recent years, hematite (α-Fe$_2$O$_3$), as an n-type semiconductor, was very used as photocatalyst for the degradation of different organic dyes such as rhodamine B (RhB), methyl orange (MO), and bisphenol A (BPA) in aqueous solution [20-27]. For example, Gandha *et al.* [20] reported the mesoporous iron oxide nanowires *via* template free approach and about 100% of RhB and MO were degraded by solar light irradiation. Kusior *et al.* [21]

*Corresponding author. E-mail: cchem2021@gmail.com

synthesized different shapes of α-Fe_2O_3 nanoparticles by an ion-mediated hydrothermal route to reach a complete degradation efficiency of RhB using Visible light irradiation by applying H_2O_2 as an electron trap. Khalaji *et al.* [23] reported photocatalytic degradation of MO dye under visible light irradiation using α-Fe_2O_3 nanoparticles prepared by a simple wet chemical precipitation route.

In this work, we describe a facile and mild two-step approach (1-wet chemical approach and 2-thermal decomposition) for the fabrication of hematite (α-Fe_2O_3) nanoparticles as photocatalyst for photodegradation of RhB and MB dyes under visible light.

EXPERIMENTAL

Materials and Methods

All materials such as $FeCl_3 \cdot 6H_2O$ (reagent grade, Sigma-Aldrich), DL-malic acid (for biochemistry, Merck), NaOH (Merck), rhodamine B (HPLC grade, Sigma-Aldrich), and methyl orange (Merck) used in this paper were purchases used without further purification. FT-IR spectra were recorded on a 5DX FTIR spectrometer (Nicolet Co., USA), using KBr pellets in the range of 4000-400 cm^{-1}. The crystal structure and phases were identified via X-ray powder diffraction (XRD) using a Bruker Advance D8 diffractometer (Cu Kα radiation, λ = 1.54056 Å). The magnetic properties were investigated using a vibrating sample magnetometer with applied magnetic field of up to 14 KOe. The morphologies of samples were recorded by scanning electron microscopy (SEM, JEOL-JSM 7600 F).

Synthesis of α-Fe_2O_3 Nanoparticles

The $FeCl_3 \cdot 6H_2O$ (0.01 mmol) as iron precursors and malic acid (0.02 mmol g) as fuel was dissolved in 30 ml distilled water by stirring and the pH value is achieved to 12 by adding 0.5 M NaOH solution and the mixture was stirred for 12 h. The brown precipitate was filtered, washed, dried, and then calcination at three different temperatures (500, 600, and 700 °C) for 3 h. The dark-red products are washed, dried, and characterized.

Photocatalytic Degradation of Methyl Orange

The photodegradation of RhB and MB dyes was studied under visible light at the natural pH. To a 50 ml of RhB and/or MB aqueous solution with initial concentration of 25 mg l^{-1}, added α-Fe_2O_3 nanoparticles and the mixture was stirred for 30 min in the dark to achieve an adsorption/desorption equilibrium, and then followed by adding 3 ml of H_2O_2 (30%). After that, the mixture was irradiated with 12 Philips TL 8w/54-7656 bulb lamps. After a given time interval, about 4 ml of the suspension was collected, filtered, and analyzed using the UV-Vis spectrophotometer. The removal percentage was calculated by the following equation, where C_o and C_t represent the initial and different reaction time absorbance of RhB and/or MB.

$$R\ (\%) = \{(C_o - C_t) \times 100\}/C_o \qquad (1)$$

Due to experimental controlling and determining the main species in the photodegradation of RhB and MB dyes, we used disodium ethylenediaminetetraacetate (EDTA), tert-butyl alcohol (TBA), and p-benzoquinone as scavengers of active h^+, $OH°$ and $O_2^{-°}$ radicals [21].

RESULTS AND DISCUSSION

Characterization of α-Fe_2O_3 Nanoparticles

FT-IR spectrum of α-Fe_2O_3 nanoparticles (Fe-500, Fe-600, and Fe-700) were shown in Fig. 1. The adsorption
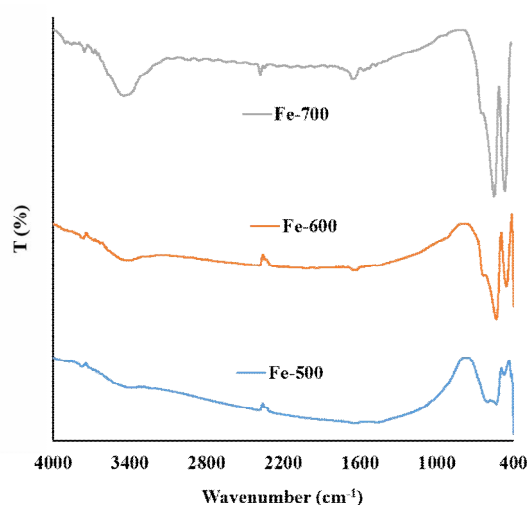

Fig. 1. FT-IR spectra of Fe-500, Fe-600, and Fe-700 nanoparticles.

bands that appeared between 450-610 cm⁻¹ are assigned to the vibration of Fe-O [23,27-31]. A broad and weak peak at about 3400 cm⁻¹ is attributed to the vibration of O-H of water adsorbed on the surface of α-Fe$_2$O$_3$ nanoparticles [23]. bands that appeared between 450-610 cm⁻¹ are assigned to the vibration of Fe-O [23,27-31]. A broad and weak peak at about 3400 cm⁻¹ is attributed to the vibration of O-H of water adsorbed on the surface of α-Fe$_2$O$_3$ nanoparticles [23].

XRD patterns of α-Fe$_2$O$_3$ nanoparticles (Fe-500, Fe-600, and Fe-700) were shown in Fig. 2. All characteristic peaks appeared at various 2θ values of $\approx$ 24.2, 33.2, 35.7, 49.5, 59.9 and 57.6 can be attributed to the 012, 104, 110, 113, 024, 116, and 018 crystalline structures corresponding to the phase-pure hexagonal structure of α-Fe$_2$O$_3$ nanoparticles with a = b = 5.038 Å, c = 13.772 Å, $\alpha = \beta = 90°$ and $\gamma = 120°$, which are in good agreement with the data of JCPDS card no. 33-0664 [23,27-31]. There are no other peaks of any impurity in the XRD pattern of α-Fe$_2$O$_3$ nanoparticles, indicating that successfully prepared high purity and well crystallized sample.

Moreover, only broad peaks were observed in the XRD pattern of Fe-500 nanoparticles, which predicted that the smaller crystalline size of Fe-500 than Fe-600 and Fe-700. The average crystallite sizes of α-Fe$_2$O$_3$ nanoparticles were calculated using the Debye-Scherrer equation, where D is crystallite size (nm), λ is the wavelength (1.54 Å), β is the FWHM of the sharp peak related to the crystal plane (104) and the θ is the Bragg's angle.

$$D = 0.94\lambda/\beta\cos\theta \tag{2}$$

The calculated average crystallite size of Fe-500, Fe-600, and Fe-700 are 25.3, 47.6, and 65.8 nm, respectively.

TEM images of α-Fe$_2$O$_3$ nanoparticles (Fig. 3) show that the particles are not in narrow distribution sizes with low agglomeration and different shapes such as spherical, cubic, and rectangle. However, the size of all particles is below 100 nm.
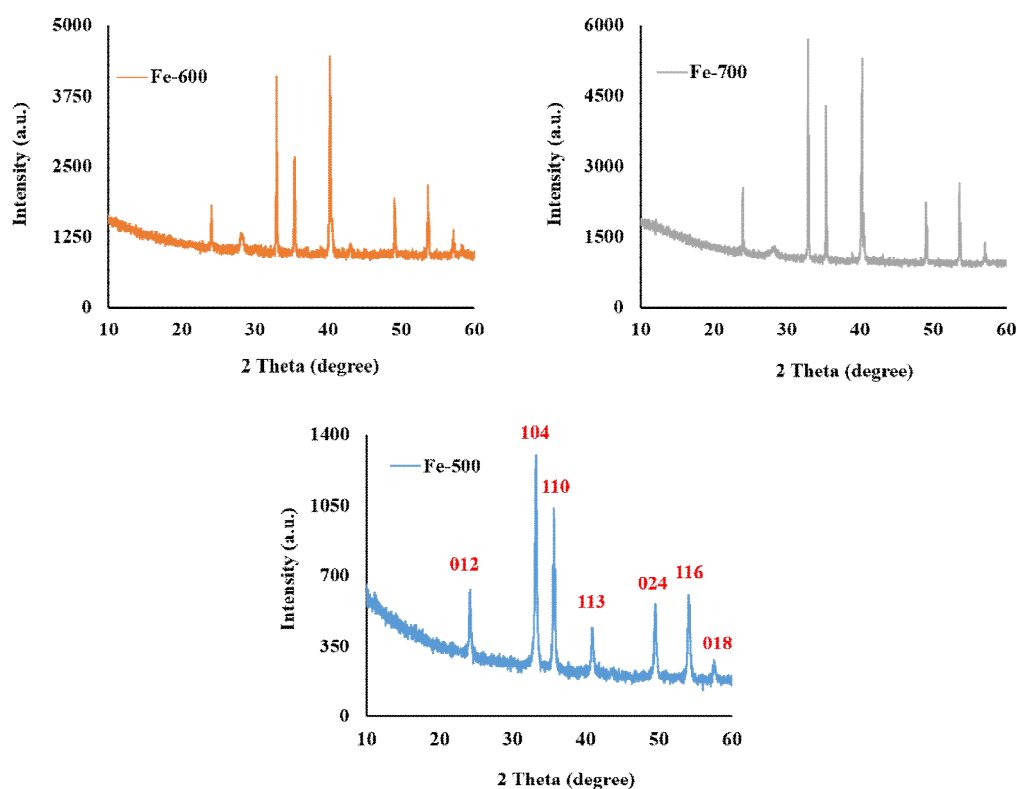

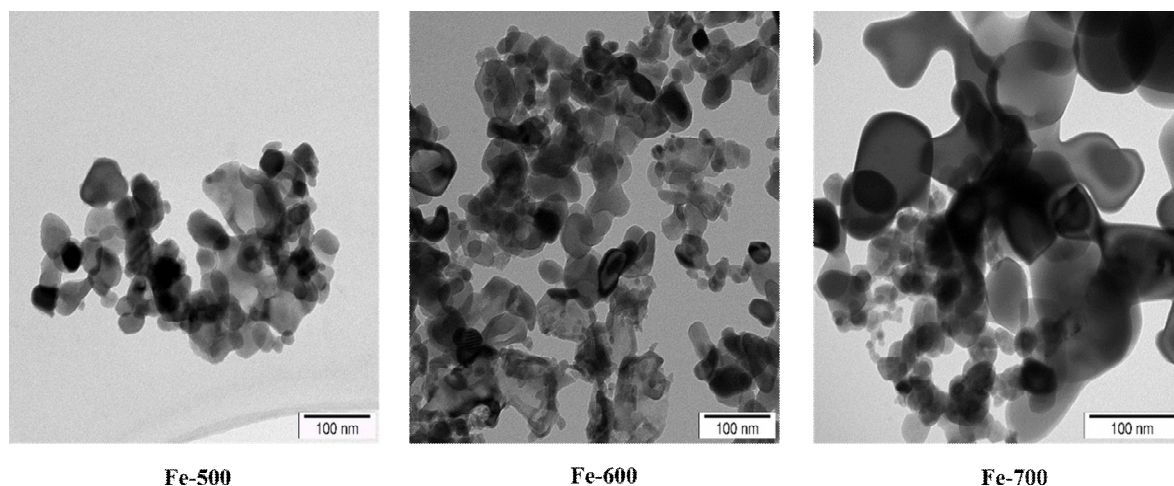**Fig. 2.** XRD patterns of Fe-500, Fe-600, and Fe-700 nanoparticles.

Fig. 3. TEM images of Fe-500, Fe-600, and Fe-700 nanoparticles.

According to TEM images, the distribution particle size histogram of Fe-500, Fe-600, and Fe-700 nanoparticles obtained, represented in Fig. 4, and exhibit a variation in particle size with the average diameter size of 25, 48, and 67 nm, respectively.

To understand the magnetic property hysteresis loops (*M-H*) of α-Fe$_2$O$_3$ nanoparticles (Fe-500, Fe-600, and Fe-700) were measured at room temperature as shown in Fig. 5. As seen in Fig. 4, saturation magnetization (M_s) of α-Fe$_2$O$_3$ nanoparticles is about 7.31, 9.25, and 11.57 emu g^{-1}, for Fe-500, Fe-600, and Fe-700, respectively, which show higher M_s than previous hematite reported [20,23,28,30] due to its smaller particles. The magnetic remanence (M_r) of α-Fe$_2$O$_3$ nanoparticles is about 0.93, 2.25, and 1.49 emu g^{-1}, for Fe-500, Fe-600, and Fe-700, respectively.

Figure 6 presents the zeta potential of Fe-500, Fe-600, and Fe-700 nanoparticles and shows that all samples have an equal isoelectric point referring to the potential zero charge (PZC) and calculated at pH ≈ 8.2. Then, the surface of samples has positive charge at pH < PZC due to the FeOH$_2^+$ groups and has negative charge at pH > PZC due to the FeO$^-$ groups [21,32].

Photocatalytic Properties

The photocatalytic activity of Fe-500 nanoparticles was studied using the degradation of RhB and MB as cationic dyes (25 mg l^{-1}) at pH > 8.2 under visible light and the
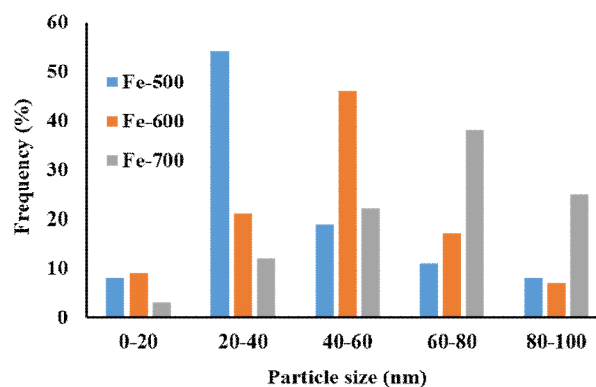

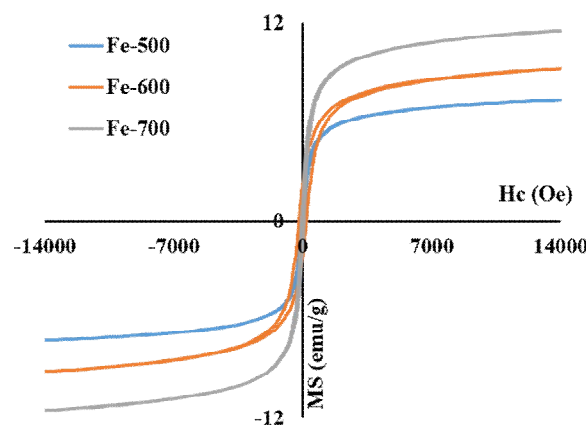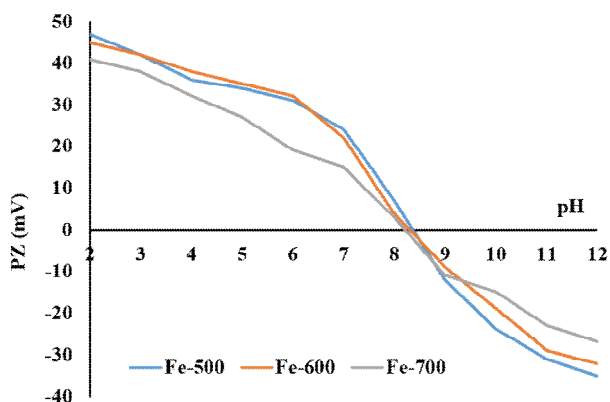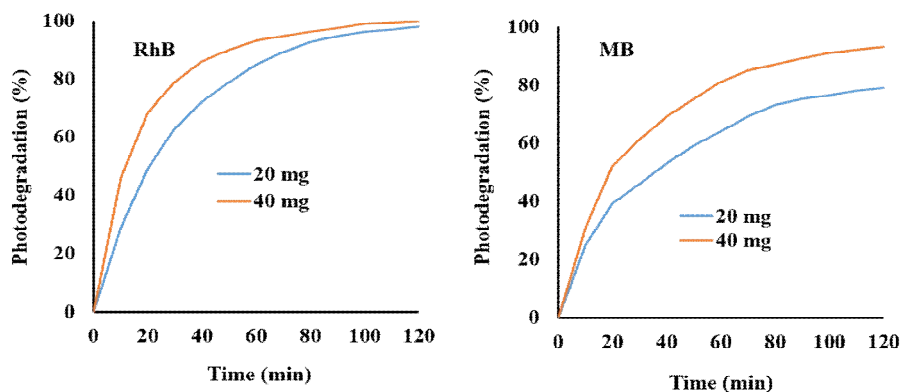**Fig. 4.** Particle size distribution histogram plots of Fe-500, Fe-600, and Fe-700 nanoparticles.

**Fig. 5.** Hysteresis loops of Fe-500, Fe-600, and Fe-700 Nanoparticles.

Fig. 6. Zeta potential of Fe-500, Fe-600, and Fe-700 nanoparticles.

effect of irradiation time (0-120 min) and the dose of catalyst (20 and 40 mg) was investigated. As seen in Fig. 7, the removal percentage of RhB photo-degradation is faster

than MB, because of the higher electrostatic interaction of RhB to negative charge of α-Fe$_2$O$_3$ nanoparticles than MB [20-24], because of more active interaction sites (N, O, COOH, and Ph rings) on the surface of RhB than MB (S and Ph rings) (Scheme 1).

The pseudo-first-order rate constant k according to the linear relationship between $\ln(C_t/C_o)$ and time (Fig. 8) was

Scheme 1. Chemical structure of RhB and MB cationic dyes
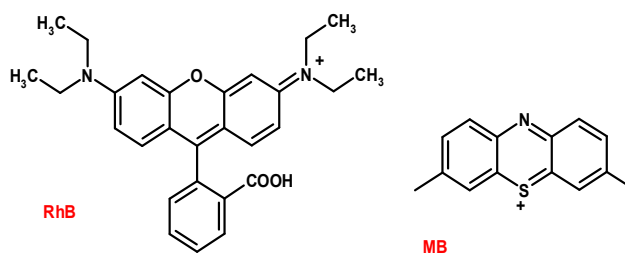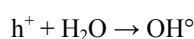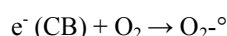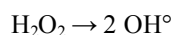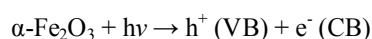

Fig. 7. The effect of irradiation time and catalyst dose on photodegradation (%) of RhB and MB dyes.
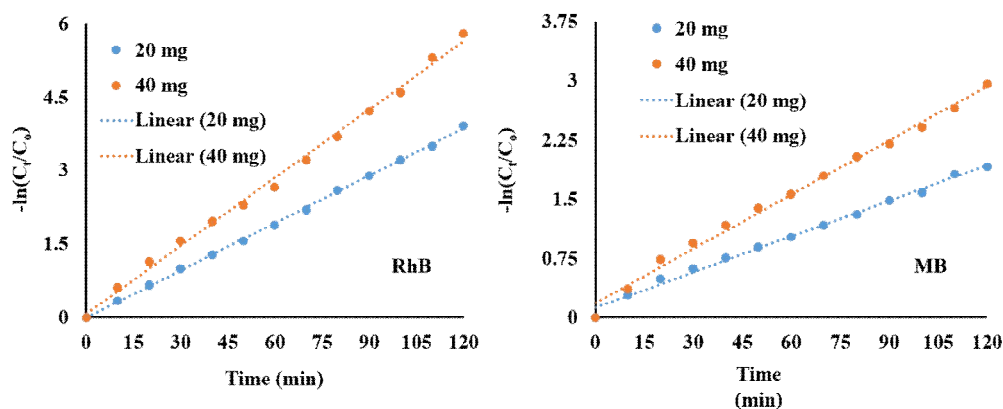
Fig. 8. Pseudo first order plots of RhB and MB dyes as a function of irradiation time and catalyst dose.

found to be 5.76×10^{-2} and 2.22×10^{-2} min^{-1}, respectively, for RhB and MO dyes [20-24].

Iron oxides (Fe$_2$O$_3$) have high intensity in the preparation of hydroxyl radical in the presence of H$_2$O$_2$ under UV-Vis light irradiation [21,33-36], due to the facile diffusion of H$_2$O$_2$ to the surface of α-Fe$_2$O$_3$ nanoparticles and causes the increase generation of hydroxyl radical (OH°) [7,21]. The mechanism of photo-degradation of RhB and MO dyes over the α-Fe$_2$O$_3$ nanoparticles can be depicted as following equations:

$$\alpha\text{-Fe}_2\text{O}_3 + h\nu \rightarrow h^+ \text{ (VB)} + e^- \text{ (CB)}$$

$$H_2O_2 \rightarrow 2 \text{ OH°}$$

$$e^- \text{ (CB)} + O_2 \rightarrow O_2\text{-°}$$

$$h^+ + H_2O \rightarrow OH°$$

RhB and/or MO + O$_2$$^-$°/OH° $\rightarrow$ degraded to safe compounds (CO$_2$ and H$_2$O)

The summary of various photocatalysts on photocatalytic degradation of RhB and MO is shown in Table 1. The comparative study shows that the as-prepared α-Fe$_2$O$_3$ nanoparticles exhibit well photocatalytic performance.

As an economical perspective and green chemistry, the reusability of as-prepared α-Fe$_2$O$_3$ nanoparticles as photocatalysts was studied under the optimized reaction conditions of RhB and MO photodegradation. Then, the

catalyst was collected using centrifugation, washed, and dried at 60 °C after each cycle. Figure 9 exhibits the photodegradation efficiency of RhB and MB using as-prepared α-Fe$_2$O$_3$ after 6 cycles. A negligible decrease in photodegradation efficiency was observed due to the loss of photocatalyst during the recycling process [6,7,37-40]. Then, the as-prepared α-Fe$_2$O$_3$ was proposed as an efficient catalyst for the degradation of RhB and MO with high stability and reusability [6,7,37-40].
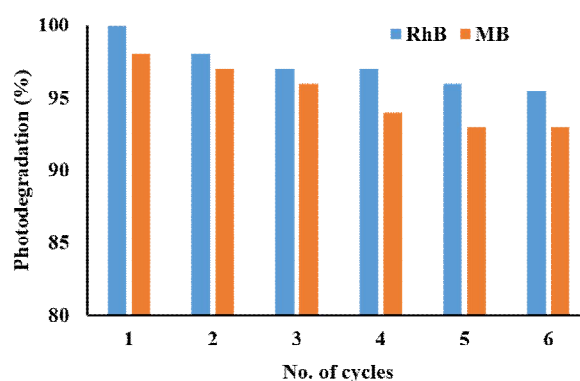
Fig. 9. Recycling experiment for as-prepared α-Fe$_2$O$_3$ Nanoparticles.

CONCLUSIONS

α-Fe$_2$O$_3$ nanoparticles were successfully synthesized, characterized, and exhibited high photocatalytic efficiency

Table 1. Comparative study of Photocatalytic Performance of Various Photocatalysts for Degradation of RhB and MB Dyes

Photocatalyst	Dye	Light source	Degradation time	Photocatalytic activity	Ref.
CeO$_2$	MB	Sunlight	70	99%	[32]
Pristine CeO$_2$	MB	UV	175	100%	[10]
CeO$_2$ nanofibers	MB	UV	60	98%	[33]
α-Fe$_2$O$_3$/ZnO	RhB	Solar	90	100%	[20]
CeO$_2$/Bi$_2$WO$_6$	RhB	Visible	120	44%	[18]
GQDs/CeO$_2$	RhB	Visible	300	96.9%	[15]
Porous Fe$_2$O$_3$	RhB	Solar	210	86.4%	[22]
α-Fe$_2$O$_3$	RhB	Visible	120	100%	This work
	MO		120	98	

for degradation of RhB and MO dyes under visible light irradiation. The degradation kinetics of RhB dye is faster than MO dye, which is completed within 60 min. This work provides a facile and low-cost route to synthesized α-Fe$_2$O$_3$ nanoparticles to photocatalytic degradation of RhB and MB dyes with photocatalytic efficiency of 100 and 98%, respectively. The as-prepared α-Fe$_2$O$_3$ nanoparticles showed superior photocatalytic activity compared with other photocatalysts under visible light and also remain stable even after 6 recycling runs.

REFERENCES

[1] Cao, Y.; Alamri, S.; Rajhi, A. A.; Anqi, A. E.; Khalaji, A. D., New chitosan Schiff base and its nanocomposite: Removal of methyl green from aqueous solution and its antibacterial activities, *Int. J. Biol. Macromol.* **2021**, *192*, 1-6. DOI: 10.1016/j.ijbiomac.2021.09.192.

[2] Kumar, S.; Krishnakumar, B.; Sobral, A. J. F. N.; Koh, J., Bio-based (chitosan/PVA/ZnO) nanocomposites film: Thermally stable and photoluminescence material for removal of organic dye, *Carbohydr. Polym.* **2019**, *205*, 559-564. DOI: 10.1016/j.carbpol.2018.10.108.

[3] Foroughnia, A.; Khalaji, A. D.; Kolvari, E.; Koukabi, N., Synthesis of new chitosan Schiff base and its Fe$_2$O$_3$ nanocomposite: Evaluation of methyl orange removal and antibacterial activity, *Int. J. Biol. Macromol.* **2021**, *177*, 83-91. DOI: 10.1016/j.ijbiomac.2021.02.068.

[4] Anitha, T.; Senthil Kumar, P.; Sathish Kumar, K., Synthesis of nano-sized chitosan blended polyvinyl alcohol for the removal of eosin yellow dye from aqueous solution, *J. Water Process Eng.* **2016**, *13*, 127-136. DOI: 10.1016/j.jwpe.2016.08.003.

[5] Madkour, M.; Allam, O. G.; Nazeer, A. A.; Amin, M. O.; Al‑Hetlani, E., CeO$_2$‑based nanoheterostructures with p–n and n–n heterojunction arrangements for enhancing the solar‑driven photodegradation of rhodamine 6G dye, *J. Mater. Sci: Mater. Elect.* **2019**, *30*, 10857-10866. DOI: 10.1007/s10854-019-01429-3.

[6] Hakimi, M.; Morvaridi, M.; Hosseini, H. A.; Alimard P., Preparation, characterization, and photocatalytic activity of Bi$_2$O$_3$-Al$_2$O$_3$ nanocomposite, *Polyhedron.* **2019**, *170*, 523-529. DOI: 10.1016/j.poly.2019.06.029.

[7] Wang, J.; Shao, X.; Zhang, Q.; Tian, G.; Ji, X.; Bao, W., Preparation of mesoporous magnetic Fe$_2$O$_3$ nanoparticle and its application for organic dyes removal, *J. Mol. Liq.* **2017**, *248*, 13-18. DOI: 10.1016/j.molliq.2017.10.026.

[8] Vatanparast, M.; Saedi, L., Sonochemical-assisted synthesis and characterization of CeO$_2$ nanoparticles and its photocatalytic properties, *J. Mater. Sci.: Mater. Elect.* **2018**, *29*, 7107-7113. DOI: 10.1007/s10854-018-8698-8.

[9] Lassoued, A.; Lassoued, M. S.; Dkhil, B.; Ammar, S.; Gadri, A., Nanocrystalline NixCo(0.5-x)Zn0.5Fe$_2$O$_4$ ferrites: fabrication through co-precipitation route with enhanced structural, magnetic and photocatalytic activity, *J. Mater. Sci: Mater. Elect.* **2018**, *29*, 7333-7344. DOI: 10.1007/s10854-018-8723-y.

[10] Majumder, D.; Chakraborty, I.; Mandal, K.; Roy, S., Facet-dependent photodegradation of methylene blue using pristine CeO2 nanostructures, *ACS Omega* **2019**, *4*, 4243-4251. DOI: 10.1021/acsomega.8b03298.

[11] Lassoued, A.; Lassoued, M. S.; Dkhil, B.; Ammar, S.; Gadri, A., Photocatalytic degradation of methyl orange dye by NiFe$_2$O$_4$ nanoparticles under visible irradiation: effect of varying the synthesis temperature, *J. Mater. Sci: Mater. Elect.* **2018**, *29*, 7057-7067. DOI: 10.1007/s10854-018-8693-0.

[12] Mahmoodi, N. M., Zinc ferrite nanoparticle as a magnetic catalyst: Synthesis and dye degradation, *Meter. Res. Bull.* **2013**, *48*, 4255-4260. DOI: 10.1016/j.materresbull.2013.06.070.

[13] Xie, T.; Liu, C.; Xu, L.; Yang, J.; Zhou, W., Novel heterijunction Bi$_2$O$_3$/SrFe$_{12}$O$_{19}$ magnetic photocatalyst with highly enhanced photocatalytic activity, *J. Phys. Chem. C* **2013**, *117*, 24601-24610. DOI: 10.1021/jp408627e.

[14] Zha, R.; Nadimicherla, R.; Guo X., Ultraviolet photocatlytic segradation of methyl orange by nanostructured TiO$_2$/ZnO heterjunctions, *J. Mater. Chem. A* **2015**, *3*, 6565-6574. DOI: 10.10399/c5ta00764j.

[15] Pei, H.; Zhang, H.; Mo, Z.; Guo, R.; Liu, N.; Jia, Q., Highly efficient photocatalytic degradation of rhodamine B by conical graphene quantum dots/cerium oxide composite, *Cer. Int.* **2020**, *46*, 3827-3836. DOI: 10.1016/j.ceramint.2019.10.106.

[16] Shan, R.; Lu, L.; Gu, J.; Zhang, Y.; Yuan, H.; Chen, Y.; Luo, B., Photocatalytic degradation of methyl orange by Ag/TiO_2/biochar composite catalysts in aqueous solution, *Mater. Sci. Semiconduct. Process.* **2020**, *114*, 105088. DOI: 10.1016/j.mssp.2020.105088.

[17] Ziaadini, F.; Mostafavi, A.; Shamspur, T.; Fathirad, F., Photocatalytic degradation of methylene blue from aqueous solution using $Fe_3O_4@SiO_2@CeO_2$ core-shell magnetic nanostructure as an effective catalyst, *Adv. Environ. Technol.* **2019**, *2*, 127-132. DOI: 10.22104/AET.2020.4137.1204.

[18] Issarapanacheewin, S.; Wetchakun, K.; Phanichphant, S.; Kangwansupamonkon, W.; Wetchakun, N., Efficient photocatalytic degradation of rhodamine B by a novel CeO_2/Bi_2WO_6 composite film, *Catal. Today* **2016**, *278*, 280-290. DOI: 10.1016/j.cattod.2015.12.028.

[19] Taghavi Fardood, S.; Moradnia, F.; Moradi, S.; Forootan, R.; Yekke Zare, F.; Heidari, M., Eco-friendly synthesis and characterization of α-Fe_2O_3 nanoparticles and study of their photocatalytic activity for degradation of Congo red dye, *Nanochem. Res.* **2019**, *4*, 140-147. DOI: 10.22036/NCR.2019.02.005.

[20] Gandha, K.; Mohapatra, J.; Hossain, M. K.; Elkins, K.; Poudyal, N.; Rajeshwar, K.; Liu, J. P., Mesoporous iron oxide nanowires: synthesis, magnetic and photocatalytic properties, *RSC Adv.* **2016**, *6*, 90537-90546. DOI: 10.1039/C6RA18530D.

[21] Kusior, A.; Michalec, K.; Jelen, P.; Radecka, M., Shaped Fe_2O_3 nanoparticles-synthesis and enhanced photocatalytic degradation towards RhB, *App. Surf. Sci.* **2019**, *476*, 342-352. DOI: 10.1016/j.apsusc.2018.12.113.

[22] Liu, X.; Chen, K.; Shim, J. J.; Huang, J., Facile synthesis of porous Fe_2O_3 nanords and their photocatalytic properties, *J. Saudi Chem. Soc.* 2015, *19*, 479-484. DOI: 10.1016/j.jscd.2015.06.009.

[23] Khalaji, A. D; Machek, P.; Jarosova, M., α-Fe_2O_3 nanoparticles: Synthesis, characterization, magnetic properties and photocatalytic degradation of methyl orange, *Adv. J. Chem. A* **2021**, *4*, 317-326. DOI: 10.22034/AJCA-2016-1268.

[24] Ye, C.; Hu, K.; Niu, Z.; Lu, Y.; Zhang, L.; Yan, K., Controllable synthesis of rhombohedral α-Fe_2O_3 efficient for photocatalytic degradation of bisphenol A, *J. Water Process Eng.* **2019**, *27*, 205-210. 10.1016/j.jwpe.2018.12.008.

[25] Munusamy, G.; Mani, R.; Varadharajan, K.; Narasimhan, S.; Munusamy, C.; Chandrasekaran, B., α-Fe_2O_3@carbon core-shell nanostructure for luminescent upconversion and photocatalytic degradation of methyl orange, *Res. Chem. Intermed.* **2020**, *46*, 715-736. DOI: 10.1007/s11164-019-03986-y.

[26] Jiang, T.; Poyraz, A. S.; Iyer, A.; Zhang, Y.; Luo, Z.; Zhong, W.; Miao, R.; El-Sawy, A. M.; Guild, C. J.; Sun, Y.; Kriz, D. A.; Suib, S. L., Synthesis of mesoporous iron oxides by an inverse micelle method and their application in the degradation of orange II under visible light and natural pH, *J. Phys. Chem. C* **2015**, *119*, 10454-10468. DOI: 10.1021/acs-jpcc.5b02057.

[27] Qiu, M.; Wang, R.; Qi, X., Hollow polyhedral α-Fe_2O_3 prepared by self-assembly and its photocatalytic activities in degradation of RhB, *J. Taiwan Inst. Chem. Eng.* **2019**, *102*, 394-402. DOI: 10.1016/j.jtice.2019.05.024.

[28] Khalaji, A. D.; Palang Sangdevini, Z.; Mousavi, S. M.; Jarosova, M.; Machek, P., Benzoic acid-functionalized α-Fe_2O_3 nanoparticles: synthesis, characterization, magnetic and optical properties, *Asian J. Nanosci. Mater.* **2021**, *4*, 137-146. DOI: 10.26655/AJNANOMAT.2.021.2.4.

[29] Mazriuaa, A. M.; Mohamed, M. G.; Fekry, M., Physical and magnetic properties of iron oxide nanoparticles with a different molar ratio of ferrous and ferric. *Egypt. J. Petrol.* **2019**, *28*, 165-171. DOI: 10.1016/j.ejpe.2019.02.002.

[30] Lassoued, A.; Lassoued, M. S.; Dkhill, B.; Ammar, S., Synthesis, photoluminescence and magnetic properties of iron oxide (α-Fe_2O_3) nanoparticles through precipitation or hydrothermal methods, *Phys. E* **2018**, *101*, 212-219. DOI: 10.1016/j.physe.2018.04.009.

[31] Pallela, P. N. V. K.; Ummey, S.; Ruddaraju, L. K.; Gadi, S.; Cherukuri, C. S.; Barla, S.; Pammi, S. V. N., Antibacterial efficiency of green synthesized α-Fe_2O_3 nanoparticles using sida cordifolia plant extract, *Heliyon* **2019**, *5*, e02765. DOI: 10.1016/j.heliyon.2019.e02765.

[32] Yavari, S., Mahmodi. N. M., Teymouri, P., Shahmoradi, B., Cobalt ferrite nanoparticles: preparation, characterization and anionic dye removal capability, *J. Tiwan Inst. Chem. Eng.* **2016**, *59*, 620-329. DOI:10.1016/j.jtice.2015.08.011.

[33] Safat, S., Buazar, F., Albukhaty, S., Matroodi, S., Enhanced sunlight photocatalytic activity and biosafety of marine-driven synthesized cerium oxide nanoparticles, *Sci. Rep.* **2021**, *11*, 14734. DOI: 10.1038/s41598-021-94327-w.

[34] Ynag, X., Liu, Y., Li, J., Zhang, Y., Effect of calcination temperature on morphology and structure of CeO_2 nanofibers and their photocatalytic activity, *Mater. Lett.* **2019**, *241*, 76-79. DOI: 10.1016/j.matlet.2019.01.006

[35] Khurram, R.; Wang, Z.; Ehsan, M. F., α-Fe_2O_3 based nanocomposites: synthesis, characterization, and photocatalytic response towards wastewater treatment, *Environ. Sci. Pollut. Res.* **2021**, *28*, 17697-17711. DOI: 10.1007/s11356-020-11778-w.

[36] Wang, Y.; Sun, Y.; Li, W.; Tian, W.; Irini, A., High performance of nanoscale Fe_2O_3 catalyzing UV-fenton under netral condition with a low stoichiometry of H_2O_2: kinetic study and mechanism, *Chem. Eng. J.* **2015**, *267*, 1-8. DOI: 10.1016/j.cej.2014.08.016.

[37] Naikwade, A. G.; Jagadale, M. B.; Kale, D. P.; Gophane, A. D.; Garadkar, K. M.; Rashinkar, G. S., Photocatalytic degradation of methyl orange by magnetically retrievable supported ionic liquid phase photocatakyst, *ACS Omega* **2020**, *5*, 131-144. DOI: 10.1021/acsomega.9b02040.

[38] Wang, H.; Xu, L.; Liu, C.; Jiang, Z.; Feng, Q.; Wu, T.; Wang, R., A novel magnetic photocatalyst $Bi_3O_4Cl/SrFe_{12}O_{19}$: Fabrication, characterization and its photocatalytic activity, *Cer. Int.* **2020**, *46*, 460-467. DOI: 10.1016/j.ceramint.2019.08.283.

[39] β-Bi_2O_3/$SrFe_{12}O_{19}$ magnetic photocatalyst; facile synthesis and its photocatalytic activity, *Mater. Technol.* **2019**, *34*, 843-850. DOI: 10.1080/10667857.2019.1638645.

[40] Malleshappa, J.; Nagabhushana, H.; Sharma, S. C.; Vidya, Y. S.; Anantharaju, K. S.; Prashantha, S. C.; Daruka Prasad, B.; Raja Naika, H.; Lingaraju, K.; Surendra, B.S., Leucas aspera mediated multifunctional CeO_2 nanoparticles: structural, photoluminescent, photocatalytic and antibacterial properties, *Spectrochim. Acta A* **2015**, *149*, 452-462. DOI: 10.1016/j.saa.2015.04.073.